Static tester for characterization of phase-change, dye–polymer, and magneto-optical media for optical data storage

Masud Mansuripur, J. Kevin Erwin, Warren Bletscher, Pramod Khulbe, Kayvan Sadeghi, Xiaodong Xun, Anurag Gupta, and Sergio B. Mendes

We have designed and built a static tester around a commercially available polarized light microscope. This device employs two semiconductor laser diodes (at 643- and 680-nm wavelengths) for the purpose of recording small marks on various media for optical data storage and for the simultaneous monitoring of the recording process. We use one of the lasers in the single-pulse mode to write a mark on the sample and operate the other laser in the cw mode to monitor the recording process. The two laser beams are brought to coincident focus on the sample through the objective lens of the microscope. The reflected beams are sent through a polarizing beam splitter and thus divided into two branches, depending on whether they are *p* or *s* polarized. In each branch the beam is further divided into two according to the wavelength. The four beams thus produced are sent to four high-speed photodetectors, and the resulting signals are used to monitor the reflectance as well as the polarization state of the beam on reflection from the sample. We provide a comprehensive description of the tester's design and operating principles. We also report preliminary results of measurements of phase-change, dye–polymer, and magneto-optical samples, which are currently of interest in the areas of writable and rewritable optical data storage.

OCIS codes: 210.4770, 120.4640.

1. Introduction

Optical data storage products encompass the range from read-only [compact disk (CD), digital versatile disk (DVD) CD-ROM, DVD-ROM] to write-once–read-many [(WORM) CD-R, DVD-R] to rewritable (magneto-optical and phase-change). The read-only media are injection molded at the factory, with the information-carrying marks embossed upon their plastic substrates. The recording process in writable and rewritable media, however, is generally a thermal process initiated by a focused laser beam. The focused beam raises the local temperature of the storage layer by a few hundred degrees Celsius, causing in the case of phase-change (PC) media a phase transition between the amorphous and crystalline states of the material and, in the case of magneto-optical (MO) media, a reversal of the magnetic moment within the heated spot. These local changes of state are accompanied by a change in either the reflectivity of the media or the state of polarization of the reflected beam. One can thus investigate the physical changes that occur during the recording and erasure processes by monitoring the reflected light.

In this paper we report the design and construction of a static tester for analyzing the recording processes in writable and rewritable media for optical data storage. The tester is built around a commercial polarized-light microscope and contains two semiconductor laser diodes operating at $\lambda_1 = 643$ nm and $\lambda_2 = 680$ nm. The two laser beams are brought to focus at the same spot on the storage layer of the media. While one laser provides the heat for raising the temperature and changing the local state of the sample, the other laser operates at a low power in the cw mode, probing the changes in the reflectivity of the sample or the state of polarization of the reflected beam without causing any significant heating of its own. Using high-speed photodetectors, we have been able to monitor the changes in the reflected light with a temporal resolution of better than 10 ns. We have thus followed the changes that take place within

The authors are with the Optical Sciences Center, The University of Arizona, Tucson, Arizona 85721. M. Mansuripur's e-mail address is masud@u.arizona.edu.

Received 26 April 1999; revised manuscript received 6 August 1999.

0003-6935/99/347095-10$15.00/0

the sample as a function of time both during the heating cycle and in the short interval immediately following the laser pulse, when the temperatures are appreciable and change is still in progress.

The paper is organized as follows. Section 2 provides a detailed description of the static tester's design and its principle of operation. Section 3 gives examples of the type of information that can be obtained from experiments on PC media; these examples shed light on the processes of crystallization, melting, and amorphization in a quadrilayer PC sample. In Section 4 we present another example of the application of the static tester, this time in analyzing the thermomagnetic recording process in MO media. Section 5 briefly describes the results of one set of measurements performed on a recordable compact disk (CD-R). Section 6 is a summary of the paper and contains a few final remarks and conclusions. The emphasis of the paper is on the design and operation of the tester, and the reported measurements are intended to serve as examples of the type of information that such a system can provide. Although some qualitative explanations of the data are given throughout the paper, a more quantitative analysis (as well as extensive measurement results) is planned for subsequent publications.

2. Design and Operation of the Static Tester

The tester is built around a commercially available polarized light microscope (Scientific Instruments, Inc., MINIMAX microscope built with Olympus components). A diagram of the complete system is shown in Fig. 1. The white-light source, the objective lens, the CCD camera, the polarizer, and the analyzer are standard elements of the microscope and were not modified by us in any way. We use the white-light source and the camera for direct observation of the recorded marks and for visual inspection of the samples. The camera also permits direct observation of the two focused laser spots, which is useful for their initial alignment. The components within the boxed region in Fig. 1 include the two lasers and the necessary optical and electronic elements for guiding their beams to the sample and for detecting the beams' properties on reflection from the sample; these items were not part of the original microscope and were added by us.

A dichroic mirror (Chroma Technology Corporation) introduces the laser beams into the main optical path of the microscope. The transmittance spectrum of the dichroic mirror at a 45° angle of incidence is shown in Fig. 2. It can be seen that the dichroic mirror is a good reflector for the two laser wavelengths (643 and 680 nm), but it is also a good transmitter for most of the rest of the white-light spectrum. The camera (Sony high-resolution 570-line RGB camera) can thus see the white-light-illuminated sample quite clearly through this dichroic mirror. The microscope's polarizer and the analyzer are needed for polarization microscopy of the MO samples. For observation of magnetic domains, for instance, we rotate the analyzer to a cross position with respect to the polarizer and then fine-tune its angular position for maximum image contrast.

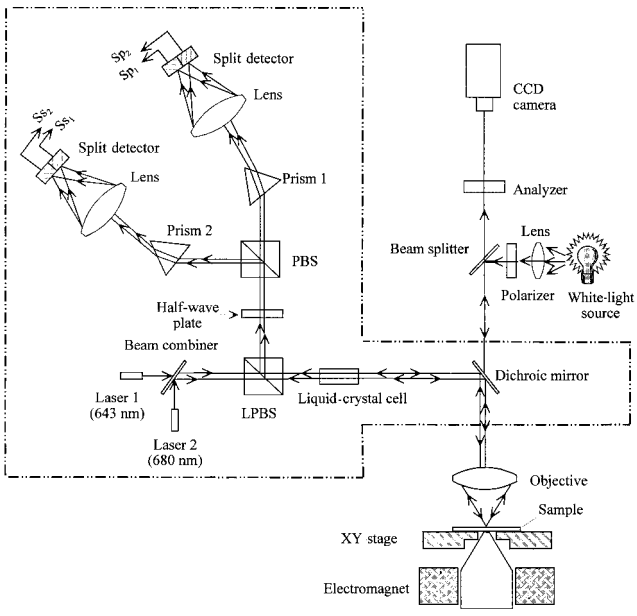

Fig. 1. Diagram of the static tester built around a polarized-light microscope. The main column of the microscope, depicted at the right, contains a white-light source, a polarizer, an analyzer, a CCD camera, and an objective lens. The sample sits atop a computer-controlled *XY* translation stage. An electromagnet is placed below the stage for measurement of MO samples. The elements within the box include two laser diodes and the necessary optics for guiding the laser beams to the sample and back to the detectors. PBS, polarizing beam splitter; other abbreviations defined in text.

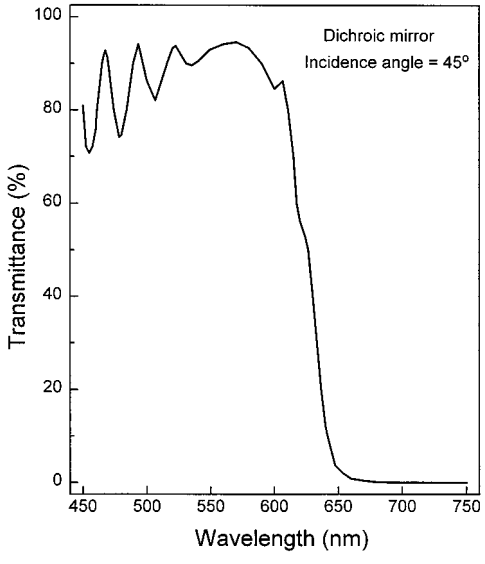

Fig. 2. Measured transmission spectrum of the dichroic mirror in the wavelength range from 450 to 750 nm at 45° angle of incidence.

A. Laser Diodes

Shown at the lower left side of Fig. 1 are two laser diodes. The beams from both lasers are linearly polarized parallel to the plane of the figure (p polarization). Each laser can be operated either in cw or in pulse mode. In the cw mode the power P_1 of laser 1 (SDL Corporation, $\lambda_1 = 643$ nm) can be adjusted continuously from 0 to 20 mW. Laser 2 (Hitachi HL 67), operating at $\lambda_2 = 680$ nm, has a cw power range from 0 to 30 mW. In the pulsed mode, both lasers can be switched with less than 5-ns rise and fall times. The maximum pulse power output of laser 1 is 40 mW; that of laser 2 is 50 mW. Both lasers have been fitted with collimating and circularizing optics (Micro-Laser Systems, Inc.). The aforementioned values of the optical power represent the lasers' raw output; the actual power available after collimation and beam shaping is only 78% of the raw power for both lasers. A feedback circuit is built into both laser drivers to maintain their cw outputs at a constant level. The feedback signal is provided by a small polarizing beam-splitter cube mounted in front of each laser diode package, which diverts ~1% of the beam to a detector in the feedback loop. Unfortunately, for the pulsed mode such feedback control of the output power is at present unavailable. As a result, the optical pulse power drifts slightly during the experiments, and the measurements need to be corrected for this variation of the laser power during the recording cycle.

The collimated and circularized beam emerging from laser 1 is approximately 4 mm in diameter; that from laser 2 is slightly larger at 5 mm. Wave-front analysis by shearing interferometry indicates that both beams are highly collimated and substantially free from aberrations, although the beam from laser 2 exhibits a small amount (~0.25λ peak to valley) of astigmatism. The beams from the two laser diodes are combined at a multilayer stack specifically designed to reflect the 680-nm line and to transmit the 643-nm line, as described below.

B. Beam Combiner

A custom-built multilayer stack brings the two laser beams together, as shown in the lower left corner of Fig. 1. Both laser beams, which impinge upon the stack at a 45° angle, are linearly polarized in the plane of incidence. The dielectric stack consists of 29 alternating layers of titania (Ti_2O_3, $n = 2.26$) and silica (SiO_2, $n = 1.45$), deposited upon a fused-silica substrate ($n = 1.45$). The various layer thicknesses of the stack are listed in Table 1, and the measured and calculated characteristics of this beam combiner appear in Fig. 3. (The stack was fabricated in a Balzers 760 electron-beam evaporator in a reactive oxygen atmosphere.) More than 98% of the output power of laser 2, incident upon the front facet of the stack, is reflected toward the sample. Laser 1 loses ~1% of its power on entering the fused-silica substrate (note that, at 45° incidence, this p-polarized beam is close to Brewster's angle), whereas another 9% is lost by reflection at the multilayer stack. All in all, the beam combiner transmits ~90% of the beam from laser 1 and reflects 98% of the beam from laser 2 toward the sample.

Table 1. Design Parameters of the 29-Layer Stack Used As a Beam Combiner in the Static Laser

Number	Medium	Refractive Index	Thickness (nm)
0	Incidence medium (air)	1.00	∞
1	Ti_2O_3	2.26	96.3
2	SiO_2	1.45	177.3
3	Ti_2O_3	2.26	100.0
4	SiO_2	1.45	125.9
5–26	Repeat bilayer 3–4	–	–
27	Ti_2O_3	2.26	100.0
28	SiO_2	1.45	191.6
29	Ti_2O_3	2.26	77.8
30	Substrate (fused silica)	1.45	∞

C. Leaky Polarizing Beam Splitter

The combined beams, now collinear and having the same p polarization (i.e., e field parallel to the plane of Fig. 1), enter a leaky polarizing beam splitter (LPBS). The LPBS (commercially available by special order from CVI) transmits 80% of the incident p-polarized light's power, reflecting the remaining 20%, which, in the forward path, is discarded. In the return path the LPBS behaves the same way, reflecting only 20% of the incident p-polarized beam toward the half-wave plate. However, the reflectance of the LPBS for s-polarized light (e field perpendicular to the plane of Fig. 1) is nearly 100%. This is important for MO samples, because the MO signal is essentially contained in the s component of the reflected polarization. In the return path this s

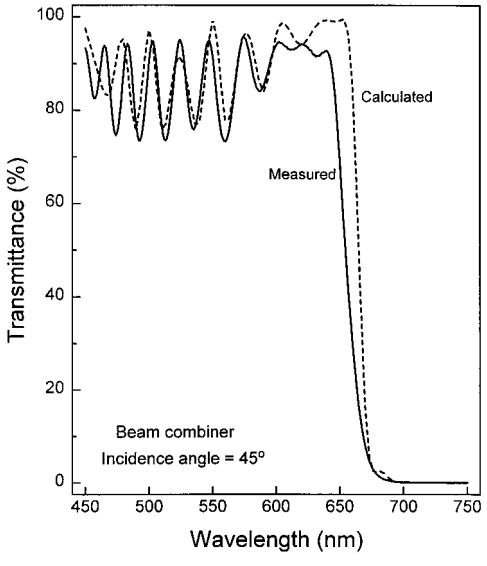

Fig. 3. Transmission spectrum of the multilayer stack used as a beam combiner at 45° angle of incidence. The calculated curve is taken from the design parameters listed in Table 1.

component is fully reflected at the LPBS and reaches the detectors. Only 20% of the returning p component from the sample goes to the detectors at this point, but the p component is needed only as a reference signal for heterodyne detection—the p component does not contain any MO information—and, therefore, no major losses occur at the LPBS. In the case of PC and WORM samples, the liquid-crystal (LC) cell described below converts the incident p-polarized light into circular polarization and, in the return path, converts the circularly polarized beam reflected from the sample into s-polarized light. Because the LPBS reflects nearly 100% of this s-polarized light toward the detectors, there are no significant losses of the optical power in the case of PC and WORM samples either.

All types of recordable and rewritable media (WORM, PC, MO) that are available at present require several milliwatts of laser power incident upon the sample in order to reach temperatures that are high enough for crystallization or melting (PC, WORM) or for magnetization reversal (MO). Given the low transmission efficiency of the microscope objectives of high numerical aperture (which is due to mismatch between the size of the laser beams and the clear aperture of the objective), it is imperative to design the rest of the optical path for maximum throughput. In our system, in the forward path the LPBS transmits ~80% of the power of each laser toward the microscope objective. The LC cell is antireflection coated and has a transmission efficiency of better than 90%, and the dichroic mirror reflects 90% of the 643-nm beam and essentially all the 680-nm beam.

D. Liquid-Crystal Phase Retarder

After the LPBS, in the forward path the system contains a LC retarder (Meadowlark Optics, LCR-100-650 cell and its B-1020 controller). For MO applications this retarder is oriented with its fast and slow axes parallel and perpendicular, respectively, to the direction of incident polarization. In the incident path the polarization, being linear and parallel to one of the axes of the LC cell, is not affected by this device. In the return path, however, the LC introduces a controlled phase shift between the p and s components of polarization. The polarization ellipticity induced in the beam by the MO sample and its substrate, if any, as well as all differential phase retardations introduced elsewhere in the system (e.g., at the dichroic mirror) can therefore be corrected by adjustment of the relative phase shift $\Delta\phi$ of the LC cell. All one needs to do in this case is to adjust the voltage control knob on the cell's controller unit to maximize the differential MO signal obtained at the detectors.

For the testing of PC and WORM media we set the relative phase delay $\Delta\phi$ of the LC cell to nearly 90° and then rotate the cell about the optical axis until its fast and slow axes are oriented at ±45° with respect to the direction of incident polarization. Of course, it is impossible to adjust $\Delta\phi$ simultaneously for both laser wavelengths, but, because λ_1 and λ_2 are close to each other, one can get nearly circular polarization for both beams out of the LC cell. In the return path, the same $\Delta\phi$ acts on the reflected beams to convert their nearly circular polarization into nearly linear s polarization (i.e., perpendicular to the plane of Fig. 1). After transmission through the LC cell in the return path, both s-polarized laser beams will be diverted at the LPBS toward the detectors.

A complicating factor in the case of PC and WORM media testing is the undesirable phase shift between r_p and r_s, the p and s reflectivities of the dichroic mirror. Ideally, the dichroic mirror must be designed to introduce no phase difference between r_p and r_s for either laser wavelength. The dichroic mirror used in our system, however, is an off-the-shelf item, which is not optimized for this particular behavior. If there is a phase difference between r_p and r_s of this mirror, it causes a departure from circular polarization of the beam incident upon the sample; moreover, in the return path it causes a reduction of the total fraction of the reflected light that would ultimately reach the photodetectors. In practice, we adjust the orientation angle as well as the retardation $\Delta\phi$ of the LC cell to minimize the backreflections from the sample into the lasers while maximizing the output of the detectors. Typically, a couple of degrees of rotation of the LC cell and a slight adjustment of $\Delta\phi$ are all that it takes to eliminate the backreflections; we estimate the dichroic mirror's phase retardation to be less than 10°. In any event, this retardation does not cause any serious difficulties for our measurements, because the polarization state of the focused spot is inconsequential in read–write experiments on PC and dye–polymer media; moreover, as far as backreflections into the lasers are concerned, the aforementioned adjustments readily solve the problem.

E. Translation Stage

The sample sits atop an XY translation stage (Prior, Inc., H-101 stage and Proscan H-128 controller), which can move under computer control in the horizontal plane in steps of 0.1 μm by as much as ±50 mm along the X axis and ±3.5 mm along the Y axis, with better than ±1.0 μm repeatability. This feature is used for scanning optical microscopy of the samples. The controlled movement of the stage is also used in experiments that require repeated measurements of the same physical quantity at different locations of the sample. In such experiments the sample moves to a new location for a fresh measurement; then the results are averaged over repeated measurements to reduce the effect of random noise. For example, in many of the measurements described in the following sections, an array of 40 marks was recorded sequentially, and the reported results are averages over these 40 points.

F. Electromagnet

Placed under the sample's stage is an electromagnet that provides the necessary magnetic field during

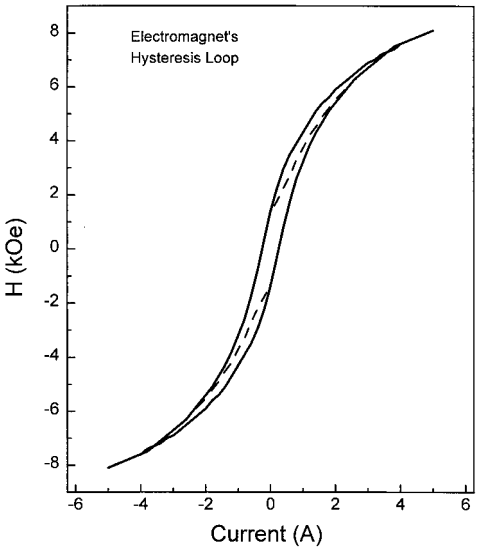

Fig. 4. Measured hysteresis loop of the electromagnet that sits beneath the sample in the system of Fig. 1. The Hall probe that we used to obtain this loop was placed in the narrow air gap between the magnet's conical pole piece and the flat iron plate (not shown) in which the magnet's external arm terminates. The horizontal axis represents the electric current applied to the coil, and the vertical axis depicts the values of the magnetic field measured by the Hall probe. The dashed curves inside the loop are the initial magnetization curves.

MO measurements. The 5-mm-diameter tip of the magnet's conical pole piece is centered directly under the focused laser spots. [Not shown in Fig. 1—but important for obtaining a large magnetic field at the sample—is an arm made from the same material (iron) as the magnet's core. The arm, attached to the bottom of the core and extending all the way to the top of the *XY* stage, provides a path of least resistance for the magnetic field, thus helping to concentrate the field in the small air gap just above the conical pole piece. Drilled in the upper end of this magnet's arm is a small hole that allows the focused beams of light to get through to the sample.] The measured field-versus-current hysteresis loop of this electromagnet is shown in Fig. 4. The maximum current supplied to the coil is ± 5.0 A, yielding a maximum magnetic field $H_{\max} = \pm 8.1$ kOe in the plane of the sample (which is also the focal plane of the objective lens).

At room temperature ($T_{\text{ambient}} = 25$ °C) the electrical resistance of the coil is 5.6 Ω, but it changes with time as the coil's temperature rises. For this reason the magnetic field is adjusted by computer control of the electrical current (rather than voltage) supplied to the coil. A complete loop scan of the field between $\pm H_{\max}$ takes anywhere from several ten seconds to a few minutes, depending on the chosen step size ΔH for the magnetic field.

G. Detection Module

The beam reflected from the sample returns through the LC cell to the LPBS and is directed toward the detectors. As we mentioned above, the LPBS reflects nearly 100% of the *s*-polarized light and only 20% of the *p*-polarized light toward the detection module. The first element in the return path after the LPBS is the half-wave plate (HWP; Special Optics, Inc., 8-9012-1/2 achromatic $\lambda/2$ plate). The bandwidth of this HWP is wide enough to allow it to function as a HWP for both $\lambda_1 = 643$-nm and $\lambda_2 = 680$-nm wavelengths. In MO applications, the HWP is used to rotate the polarization until the light is nearly equally split between the two detection channels. For PC samples the HWP is not necessary, but it may be used to control the amount of light that enters the desired channel. The polarizing beam splitter (Newport Corporation, part 05-FC-16-PB.3) immediately after the HWP sends the component of polarization parallel to the plane of the diagram straight through, but it reflects the perpendicular polarization toward the channel on the left.

The two beams exiting the polarizing beam splitter go through identical prisms (Melles-Griot 01-PEH-010/78 equilateral flint prism, 25 mm). The dispersion of these prisms is large enough to separate the two wavelengths. Emerging from each prism are two beams with wavelengths λ_1 and λ_2 that have an angular separation of $\sim 0.28°$. In each channel a 63.5-mm focal-length lens (Newport PAC531-AR.14) focuses the two beams on the separate halves of a split photodetector (Hamamatsu Si P–I–N photodiode 56058. This is actually a quad detector, in which each individual rectangular detector is 300 μm × 600 μm in size and the gap width between adjacent cells is 10 μm. We use only two of the four detectors in each channel, choosing the diagonal pair for maximum separation and minimum cross talk.) The focused spots are ~ 25 μm in diameter, and their center-to-center spacing is ~ 300 μm.

We thus collect four signals, S_{p1}, S_{p2}, S_{s1}, and S_{s2}, out of the two split detectors. Here the subscripts *s* and *p* refer to the state of polarization of the beam that emerges from the HWP and the subscripts 1 and 2 refer to wavelengths λ_1 and λ_2, respectively. The individual detectors have an efficiency $\eta \sim 0.5$ mA/mW. The gain of the amplifiers for the detectors of the λ_1 line is $G_1 = 50$ V/mA; that of the λ_2 line is $G_2 = 14$ V/mA. All amplifiers have a 160-MHz bandwidth. By forming the various sums and differences of the electronic signals one obtains the total reflectance of the sample as well as the differential MO signal. (The reflectances of the various samples are calibrated against a polished silicon surface's reflectivity, which is used as a reference surface.) For PC and WORM measurements we usually adjust the HWP to send all the light through the polarizing beam splitter. In this case S_{p1} is proportional to the reflectivity of the sample at λ_1 and S_{p2} represents the reflectivity at λ_2. For MO measurements, the fast (or slow) axis of the HWP is rotated by 22.5° from the plane of Fig. 1, sending equal amounts of the two components of polarization to each detector. In this case the normalized differential signals are $(S_{p1} - S_{s1})/(S_{p1} + S_{s1})$ for λ_1 and $(S_{p2} - S_{s2})/(S_{p2} + S_{s2})$ for λ_2. The normalized differential signals are propor-

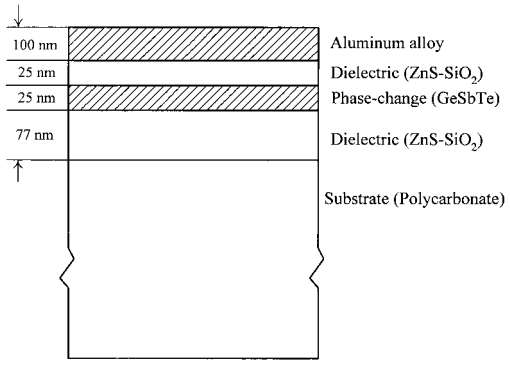

Fig. 5. Quadrilayer stack consisting of a thin film of $Ge_2Sb_2Te_5$ PC material sandwiched between two dielectric layers and capped with an aluminum alloy film. The laser beams must be focused upon the PC layer through the substrate. The results of measurements of this sample appear in Figs. 6 and 7.

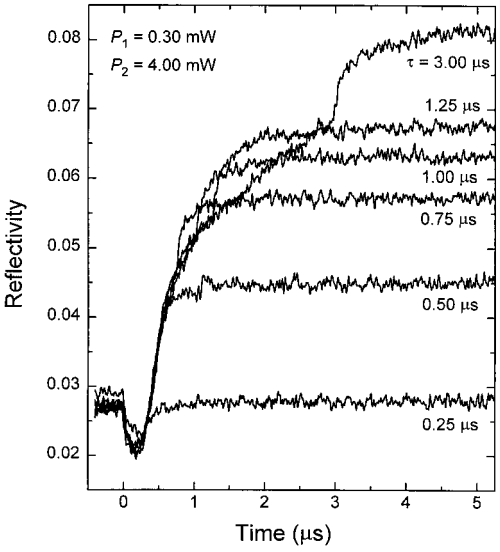

Fig. 6. Plots of reflectivity versus time during local crystallization of the as-deposited amorphous PC film encapsulated in the quadrilayer stack of Fig. 5. The pulsed beam from laser 2 had a peak power of 4.00 mW, but its duration τ was fixed at different values for the various curves shown. The cw power of laser 1 was fixed at 0.3 mW. Both beams were focused on the same spot on the sample through a 0.6-N.A. objective, which was corrected for the 1.2-mm thickness of the sample's substrate.

tional to the polarization rotation angle at the sample (i.e., Kerr angle in the case of MO media), but one must be careful to account for the reduced value of the p component of polarization at the LPBS.[1,2]

H. Calibration

We performed several measurements on aluminized mirrors and polished silicon substrates to calibrate the system. Both aluminum and silicon have high thermal conductivities and, therefore, the laser beams were not expected to create substantial temperature profiles in them. We used the reflected light from these calibration samples to determine the shape of the laser pulse and to establish the relationship between the measured voltage at the detectors and the actual reflectance of the sample. The cross talk between adjacent detectors was also measured and found to be at acceptable levels.

3. Measurements on Phase-Change Sample

We made these measurements on the quadrilayer sample depicted in Fig. 5 by focusing the two laser beams on the PC layer through the sample's substrate. The sample, deposited upon a 1.2-mm-thick polycarbonate substrate, had a 77-nm-thick ZnS–SiO_2 dielectric layer, a 25-nm layer of $Ge_2Sb_2Te_5$, another 25-nm layer of ZnS–SiO_2, and a 100-nm-thick layer of aluminum alloy. The PC layer was initially in the as-deposited amorphous state. The microscope objective (Olympus FCplan-FL 40× objective and appropriate compensator cap such as P1.1 ± 0.5) used in these experiments had a numerical aperture of 0.6 and was corrected for the thickness of the substrate through which the light had to pass to reach the PC layer.

Figure 6 shows the results of measurements performed on the as-deposited amorphous $Ge_2Sb_2Te_5$ film. Laser 2 was pulsed at $P_2 = 4$ mW peak power with a variable pulse width, and laser 1 operated cw at $P_1 = 0.3$ mW. P_1 is small enough that its thermal effects on the sample during these measurements may be ignored. The six curves in Fig. 6 correspond to six different pulse widths, as follows: $\tau = 0.25$, 0.50, 0.75, 1.00, 1.25, 3.00 μs. In each case the change in the reflectivity of the sample versus time, as measured by the cw laser, is shown. In none of these cases do we believe that the sample reaches the melting point temperature ($T_{\text{melt}} \approx 600$ °C); therefore the observed phenomena are due solely to the crystallization of the amorphous film as well as the (reversible) change of the material's optical constants with temperature.

The reflectivity starts at the amorphous level of approximately 3% and then drops by ~1% in the early phase of the experiment. This drop is believed to be due to a reversible change of the optical constants of the PC layer with the rising temperature, but its cause certainly warrants further investigation.[3] The temperature rise is fairly rapid, so after ~200 ns the reflectivity begins to increase. This increase is caused by crystallization of the sample under the focused 680-nm laser beam. For the shortest pulse there is hardly any crystallization, and the reflectance appears to return to its original value after laser 2 is turned off. (Random noise and statistical variations among the results of repeated experiments limit the accuracy of these reflectance measurements to ~0.25%.) The longer pulses show a rapid crystallization at first, followed by a period of slower crystallization. This behavior is in part a result of the light absorption and thermal diffusion processes that raise the temperature rapidly at first and then slow down as the thermal diffusion process takes over. The complete explanation of the observed behavior is much more complicated, of course, because the effects

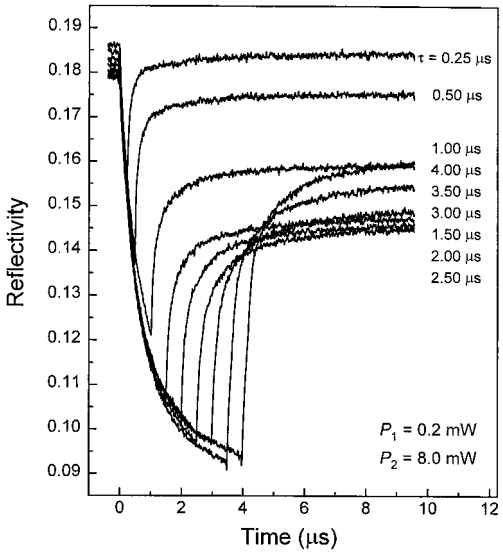

Fig. 7. Plots of reflectivity versus time during local melting and subsequent quenching of the precrystallized PC film encapsulated in the quadrilayer stack of Fig. 5. The pulsed beam from laser 2 had a peak power of 8.0 mW, but its duration τ was fixed at different values for the various curves shown. The cw power of laser 1 was fixed at 0.2 mW. Both beams were focused on the same spot on the sample through a 0.6-N.A. objective, which was corrected for the 1.2-mm thickness of the sample's substrate.

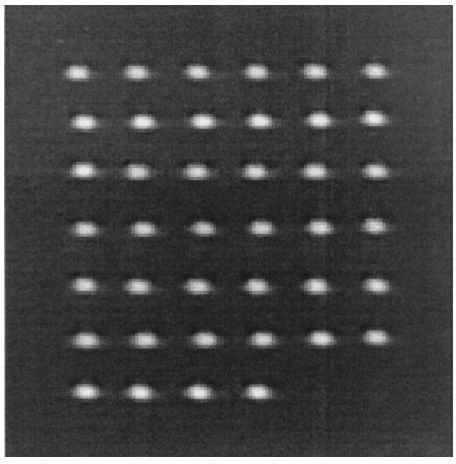

Fig. 8. Photograph of the recorded marks on a PC sample, as seen through the CCD camera. These crystalline marks were written upon an as-deposited amorphous film with 7.0-mW, 2.0-μs pulses from laser 2. The center-to-center spacing between adjacent marks is 6 μm.

of diffraction from the growing mark boundary, the changing of optical constants with temperature, the convolution of the read-beam intensity with the reflectance of the sample within the illuminated area, and the changing probabilities of nucleation and growth with temperature must also be taken into account. At the end of the pulse in each case we observe a rapid increase of ~1% in reflectivity; again, this is most likely a result of the PC film's cooling down and of the consequent change in its optical constants, although other possibilities (e.g., rapid recrystallization of small molten pools) cannot be ruled out.

Another example of measurements of the same PC sample is shown in Fig. 7. Here the sample was first crystallized on a fairly large area (approximately 30 μm × 30 μm), using the computer-controlled scanning capability of the *XY* translation stage. For this large-area crystallization the 680-nm laser was used in multiple scans at the cw power of P_2 = 2.0–3.0 mW. Afterward, we recorded small marks on this crystallized area of the sample by pulsing laser 2 at a peak power of P_2 = 8.0 mW for several pulse widths, τ = 0.25, 0.50, 1.00, 1.50, 2.00, 2.50, 3.00, 3.50, 4.00 μs. Laser 1, operating in the cw mode at P_1 = 0.2 mW, was used to monitor the local melting and the subsequent quenching of the sample.

The nine curves in Fig. 7 show the results of these measurements obtained for each of the nine different pulse widths. The initial reflectivity before the start of the pulse at t = 0 is slightly greater than 18%. (The curves are slightly displaced in the vertical direction for the clarity of viewing. When the same experiment is repeated over and over again, the statistical variation of reflectivity is found to be slightly less than 0.25%.) For the shortest pulse there is some change in the optical constants and probably a small amount of melting, causing a 2% drop in reflectivity, but then the signal increases to its original value after the end of the pulse, indicating that the changes in the optical constants are reversible and that the molten area, if any, has fully recrystallized by the time the pulse has terminated.

For the τ = 0.5 μs pulse the reflectivity rises at the end of the pulse, but, at the end of the measurement period (t = 10 μs), the reflectivity has not reached its original value. This result indicates that there has been some melting during the pulse but that, when the pulse was turned off, the molten area crystallized only partially, probably starting at the outer rim of the molten pool and moving inward. At the end, the molten pool did not fully recrystallize, and a small amorphous mark was left at its center. In fact, visual inspection of the sample under the microscope shows a small dark spot in the middle of the recording area. Similar explanations apply to longer pulses, but in these cases the final amorphous marks are seen (both visually and from the final value of reflectivity in Fig. 7) to be larger. Note that for the three pulses that have the longest duration (namely, those with τ = 3.00, 3.50, 4.00 μs) the final reflectivity at t = 10 μs is progressively larger than those obtained with shorter pulses (e.g., τ = 1.50, 2.00, 2.50 μs). This may be an indication that the radial heat diffusion has broadened the thermal profiles within the PC layer induced by longer pulses, in consequence of which the cooling process has slowed down. Slow cooling then results in more crystallization, leaving smaller amorphous marks at the end of the cycle.[4–6]

Figure 8 is a photograph of the recorded marks on the PC sample as seen through the CCD camera. These crystalline marks were recorded on an as-

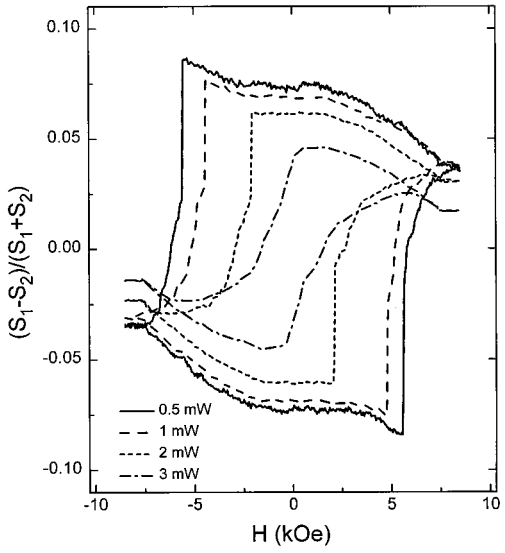

Fig. 9. Kerr hysteresis loops measured on a front-surface quadrilayer MO sample by the cw beam from laser 1 while laser 2 was turned off. These four loops were obtained at different values of beam power P_1 (measured at the sample's surface). The magnetic field was scanned between ± 8.1 kOe in steps of 50 Oe. The beam was focused on the magnetic layer of the sample through a 0.6-N.A. objective. The LC cell's phase shift $\Delta\phi$ was adjusted for the maximum Kerr signal, i.e., the loop height.

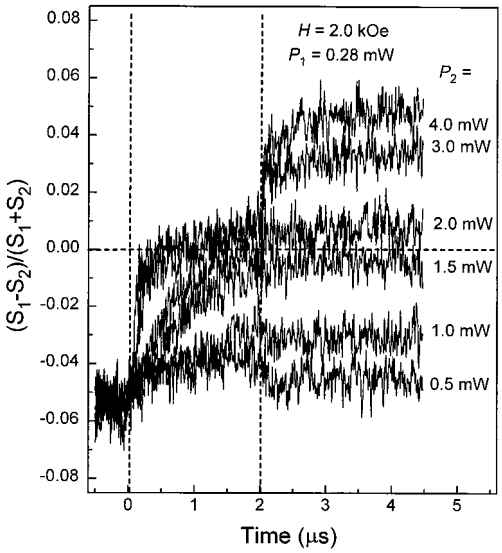

Fig. 10. Plots of Kerr signal versus time during the process of thermomagnetic recording on the same quadrilayer MO sample as used in Fig. 9. The cw probe beam from laser 1 was set at the low power level of $P_1 = 0.28$ mW. The magnetic field was fixed at $H = -2$ kOe, and laser 2 was pulsed for a $\tau = 2$ μs duration. The various curves shown correspond to different pulse power levels P_2, as indicated on each curve. Both laser beams were focused on the same spot on the sample through a 0.6-N.A. objective. The large bandwidth of the detector module and the small magnitude of the differential MO signal are responsible for the noisy appearance of these plots.

deposited amorphous region with 7.0-mW, 2.0-μs pulses from laser 2; the spacing between adjacent marks is 6 μm. The slight elongation of the marks in the horizontal direction is caused by the undercorrected astigmatism of the laser beam. Although our qualitative analysis of the results presented in this paper is not influenced by this slight ellipticity of the marks, for accurate quantitative analysis one must either correct the residual astigmatism or take the shape of the recording focused spot into account.

4. Magneto-Optical Measurements

Figure 9 shows several hysteresis loops measured on a front-surface quadrilayer MO sample with the aid of our static tester. The sample consisted of a polycarbonate plastic substrate coated with a 100-nm-thick aluminum alloy layer, a 50-nm-thick layer of SiN, a 25-nm-thick layer of amorphous TbFeCo, and a 80-nm-thick layer of SiN as the top layer. The magnetic film's composition is such that its compensation point temperature T_{comp} is somewhat below the room temperature T_{ambient}. As a result, the coercivity H_c of the sample is a decreasing function of temperature for $T > T_{\text{ambient}}$.

Laser 2 was turned off during this experiment, and the 643-nm beam from laser 1 was focused through a 0.6-N.A. objective lens from the top of the sample onto the magnetic layer. (Because this is a front-surface sample, the objective lens does not need correction for the substrate.) The four hysteresis loops of Fig. 9 were measured at four separate locations on the sample, each loop corresponding to a different laser power P_1, ranging from 0.5 mW for the outer loop to 3 mW for the inner loop. Because the focused beam raises the local temperature of the sample, the coercivity drops with the increasing laser power, as is evident from the loops of Fig. 9. The loops are much more complex than the loops usually measured on MO media, because, unlike conventionally measured loops, these loops represent a small region of the sample under a nearly Gaussian temperature distribution. (The temperature profiles created by the focused beam from laser 1 are expected to be in steady state during these measurements.) Some of the loops show discrete jumps, indicating the release of trapped domain walls at the corresponding value of the magnetic field. The decline of the MO signal at large values of H is not understood at the present time. It could be caused by the Faraday effect of the objective lens under the applied magnetic field, or it could arise from an in-plane magnetized film that is formed (as a result of oxidation or aging) at the interface between the magnetic layer and its neighboring dielectric layers.

In another experiment on the same MO sample, the magnetic field was fixed at $H = 2.0$ kOe, and both lasers were turned on. The two focused spots were coincident, with the 680-nm laser being pulsed for 2.0 μs while the 643-nm laser was operating in the cw mode at $P_1 = 0.28$ mW. Six measured curves for six different values of pulsed laser power P_2 are shown in Fig. 10. In all cases the sample was originally saturated under a large magnetic field. The direction

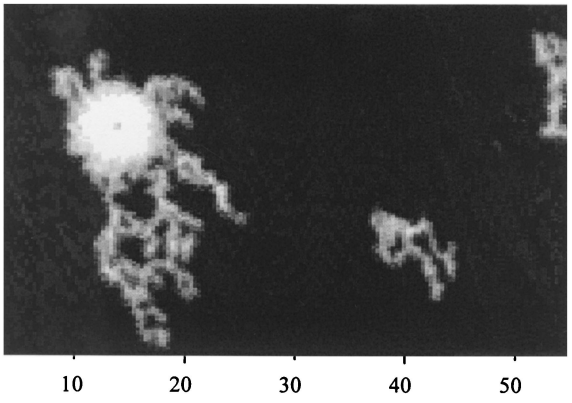

Fig. 11. Scanning polarization micrograph of a thermomagnetically recorded domain after it has been expanded under a magnetic field just below the sample's coercivity. Many branches appear on the periphery of the domain, and new nucleation centers develop in other regions of the sample.

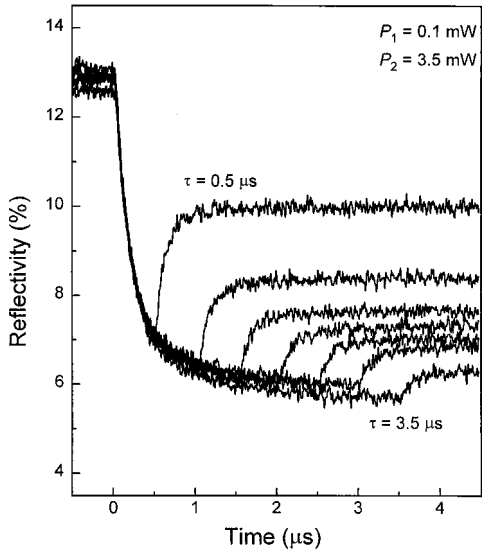

Fig. 12. Plots of reflectivity versus time during local melting–ablation of the dye layer of a commercial CD-R disk. The pulsed beam from laser 2 had a peak power of 3.5 mW, but its duration τ was fixed at different values for the various curves (τ = 0.5–3.5 μs in steps of 0.5 μs). The cw probe power was fixed at P_1 = 0.1 mW. Both beams were focused on the same spot on the disk through a 0.6-N.A. objective, which was corrected for the 1.2-mm thickness of the sample's substrate.

of the field was then reversed, and its magnitude was fixed at H = 2.0 kOe. The pulsed laser was turned on at t = 0. When the pulse power is low (i.e., P_2 = 0.5 mW or P_2 = 1.0 mW), the MO signal monitored by the cw laser does not change much. There seems to be a small amount of heating, which reduces the MO Kerr signal, but, as soon as the pulsed laser is turned off at t = 2 μs, the signal recovers its original value. At higher pulse powers, such as P_2 = 1.5 mW and P_2 = 2.0 mW, the central region of the focused beam succeeds in raising the sample's temperature enough to cause a magnetization reversal. The reversed domain, however, is small, and the net Kerr signal at the end of the pulse is close to zero. This signal level also persists after the pulse has been turned off, presumably because the up- and down-magnetized regions of the sample under the focused beam cancel each other out. At higher pulse powers, namely, P_2 = 3.0 mW and P_2 = 4.0 mW, the reversal occurs early during the pulse period, and the signal remains at zero throughout the entire pulse because the heated spot is above the Curie temperature of the magnetic layer. As soon as the pulse is turned off, however, the temperatures decline and the MO signal recovers its original value, albeit with the opposite sign, as expected.[7–9]

A polarized-light scanning micrograph of a magnetic domain is shown in Fig. 11. The domain was recorded thermomagnetically and was subsequently subjected to a magnetic field just below the sample's coercivity. Dendritic growth from the boundary of the recorded domain and formation of nuclei of reverse magnetization in nearby regions are clearly observed in this photomicrograph. The scanning step size was 0.1 μm, and the laser power was kept low to prevent it from heating the sample.

5. Measurements on a CD-R Disk

Figure 12 shows the results of a series of measurements of a commercial CD-R disk. In its native state the dye layer of the disk is highly reflective, but, in the process of recording, the region exposed to the focused spot ablates and its reflectivity drops sharply. The CD-R media are optimized for operation at λ = 780 nm, so at our wavelengths of 643 and 680 nm their reflectivity and absorption are quite different from the optimal values. Nonetheless, the thermal processes underlying mark formation are the same and, therefore, the results presented in Fig. 12 are useful. The seven curves shown in this figure were obtained at different locations on a flat (i.e., nongrooved) region of the disk. The probe laser power was P_1 = 0.1 mW, the pulse power was P_2 = 3.5 mW, and the pulse duration τ varied from 0.5 to 3.5 μs in steps of 0.5 μs. The shapes of these curves are self-explanatory in that they show the drop in reflectivity during the pulse and the partial recovery after the pulse. Moreover, the change in reflectivity after the end of the pulse is seen to be smaller for wider pulses. Explaining the underlying physical processes, however, is much more complicated and requires a thorough understanding of the laser-induced melting and ablation of the dye layer in conjunction with the local melting, possible evaporation, and final deformation of the substrate.[10,11] Such an explanation requires computer simulations of the various thermochemical and rheological processes in the media under the focused laser spot, which is obviously beyond the scope of the present paper. Nonetheless, measurements such as those depicted in Fig. 12 can provide valuable insight and qualitative understanding of the recording mechanism in CD-R media.

6. Concluding Remarks

We have built a static tester for the magneto-optical, phase-change, and write-once–read-many media used in optical data storage. The tester has been used to monitor the changes in the state of the sample during local heating and cooling by a focused laser beam. Inasmuch as the details of the thermomagnetic process in MO media as well as the phase transformation processes in PC and WORM media are essential for determining the final shape and size of the recorded marks as well as the speed of recording and erasure, this type of measurement is expected to be valuable for developers of future generations of optical data storage media and systems.

Thanks are due to T. Ohta, K. Nagata, and N. Miyagawa of the Matsushita Electric Company of Japan for providing the PC sample used in these studies. The MO sample was provided by Chung-Hee Chang of Seagate Media Research Center, Fremont, California, to whom we are also grateful. This research has been sponsored by the Optical Data Storage Center of the University of Arizona in Tucson and in part by a grant from the U.S. Department of Commerce's National Institute of Standards and Technology under Advanced Technology Program award 70NANB7H3054.

References and Notes

1. T. W. McDaniel and R. H. Victora, eds., *Handbook of Magneto-optical Recording* (Noyes, Westwood, N.J., 1997).
2. M. Mansuripur, *The Physical Principles of Magneto-optical Recording* (Cambridge U. Press, London, UK, 1995).
3. Reversibility of the initial decline in the reflectivity curves of Fig. 6 may be inferred from the $\tau = 0.25$ μs curve; it was also confirmed by our numerous other short-pulse experiments on the same sample. At $P_2 = 4$ mW and $t = 100$ ns the temperature rise at the center of the focused spot is estimated to be ~300 °C, which is large enough to cause changes in the electronic band structure and consequently to modify the optical constants of the sample.
4. S. R. Ovshinsky, "Reversible electrical switching phenomena in disordered structures," Phys. Rev. Lett. **21,** 1450–1453 (1968).
5. J. Feinleib, J. deNeufvile, S. C. Moss, and S. R. Ovshinsky, "Rapid reversible light-induced crystallization of amorphous semiconductors," Appl. Phys. Lett. **18,** 254–257 (1971).
6. T. Ohta, M. Takenaga, N. Akahira, and T. Yamashita, "Thermal change of optical properties in some sub-oxide thin films," J. Appl. Phys. **53,** 8497–8500 (1982).
7. D. Chen, G. N. Otto, and F. M. Schmit, "MnBi films for magneto-optic recording," IEEE Trans. Magn. **MAG-9,** 66–83 (1973).
8. Y. Mimura, N. Imamura, and T. Kobayashi, "Magnetic properties and Curie point writing in amorphous metallic films," IEEE Trans. Magn. **MAG-12,** 779–781 (1976).
9. S. Yonezawa and M. Takahashi, "Thermodynamic simulation of magnetic field modulation methods for pulsed laser irradiation in magneto-optical disks," Appl. Opt. **33,** 2333–2337 (1994).
10. J. J. Wrobel, A. B. Marchant, and D. G. Howe, "Laser marking of organic films," Appl. Phys. Lett. **40,** 928–930 (1982).
11. E. Hamada, T. Fujii, Y. Takagishi, and T. Ishiguro, "Recording process of recordable compact disc," in *Optical Data Storage*, D. B. Carlin and D. B. Kay, eds., Proc. SPIE **1663,** 443–446 (1992).